JOURNAL OF COLLOID AND INTERFACE SCIENCE **208,** 430–438 (1998)
ARTICLE NO. CS985794

Adsorption/Desorption Kinetics of MoO_4^{2-} onto γ-Al_2O_3 by the Pressure-Jump Technique

Chung-Hsin Wu, Cheng-Fang Lin,[1] Shang-Lien Lo, and Tatsuya Yasunaga[2]

Graduate Institute of Environmental Engineering, Natural Taiwan University, Taipei, 106, Taiwan

Received April 22, 1998; accepted August 6, 1998

The kinetics and mechanisms of molybdate adsorption/desorption at the γ-Al_2O_3/water interface were studied by using the pressure-jump apparatus with conductivity detection at 298 K. A double relaxation was observed due to the adsorption/desorption process. Adsorption data and triple-layer model (TLM) simulation results suggest the formation of both mono- and bidentate inner-sphere complexes ($SMoO_4^-$ and S_2MoO_4) at the γ-Al_2O_3 surface. The intrinsic equilibrium constants (K_{eq}^{int}) of the complexes were $10^{6.5}$ M^{-2} and 10^{16} M^{-4}, respectively. Based on the relaxation theory and combined results of TLM simulation, a two-step process is proposed. The first step (k_1, k_{-1}) is the formation of an ion-pair complex through the electrostatic attraction between the reacting surface sites and MoO_4^{2-} and H^+. The second step (k_2, k_{-2}) involves a ligand exchange process, whereby one water molecule is replaced by one adsorbed MoO_4^{2-} from the surface. The values of adsorption and desorption rate constants in the MoO_4^{2-}/γ-Al_2O_3 system were determined to be $k_1^{int} = 5.23 \times 10^6$ M^{-2} s^{-1}, $k_{-1}^{int} = 2.41 \times 10$ s^{-1}, $k_{-2}^{int} = 1.74$ s^{-1}, and $k_{-2}^{int} = 3.26 \times 10^{-1}$ s^{-1}. The intrinsic equilibrium constant from kinetic measurements (K_{kin}^{int}) was 10^6 M^{-2}, which was similar to the intrinsic equilibrium constant (K_{eq}^{int}), $10^{6.5}$ M^{-2}, from the equilibrium studies. © 1998 Academic Press

Key Words: **MoO_4^{2-}; γ-Al_2O_3; TLM; pressure-jump; intrinsic adsorption/desorption rate constant.**

INTRODUCTION

Molybdenum is an essential trace element for protein synthesis and oxidation in human metabolism (1). In practical uses, molybdenum is a critical component of making high-strength steels, which contain molybdenum some 0.25% to 8% by weight (1). Molybdenum is also involved in the production of heat- and corrosion-resistant alloys, screen materials in electron tubes, and electrode materials for electrically heated furnaces (2). Pure molybdenum metal is not found in nature and cannot be obtained without a separation process. Rather, its free element can be extracted from wulfenite, which is lead molybdate. Like other transition metals, molybdenum and/or molybdate compounds are toxic materials to grazing animals as well as humans (3); the degree of toxicity of molybdenum and/or molybdate compounds ranks between Zn(II) and Cr(III) compounds. These toxic molybdenum and molybdate compounds are commonly detected as soluble molybdate in the hydrosphere and as the adsorbed form on Fe and/or Al hydroxide/oxide in the soil.

For the past two decades, the fate and distribution of environmental trace elements have been studied extensively. The surface complexation model of Stumm *et al.* (4) elucidated that cations react with surface hydroxyl groups and exchange for H^+, whereas anions react with surface hydroxyl groups and exchange for OH^-. The equilibrium conditions of interfacial complexation reactions have been further quantified by the triple-layer model (TLM) of Davis and Leckie (5) and later modified by Hayes and Leckie (6). The TLM provides an interpretation of experimental data that is closely related to the real phenomena; however, it does not give direct evidence to verify the reaction mechanisms. Though many studies have addressed the importance of Fe and Al hydroxide/oxide on regulating the transport of environmental pollutants, work on molybdate association with mineral surfaces is very limited.

Pankow and Morgan (7) stated that a natural system may never reach an equilibrium state and that kinetic processes are more important than equilibrium in understanding pollutant distributions. Kinetic information also provides insight into the intrinsic interaction pathways of the adsorption systems. Traditionally, batch and flow methods are commonly applied to kinetic work on cation as well as anion adsorption/desorption on minerals (8). Because reaction changes cannot be detected as rapidly as adsorption proceeds, batch and flow kinetic work can only provide apparent (or the overall) kinetic rate data but not intrinsic rate information, the later can be used for verifying the reaction mechanisms. In 1979, a research team led by Yasunaga started to investigate the adsorption kinetics of divalent cations (Pb, Zn, Cu, and Cd) on Al oxides using a relaxation-based technique involving the pressure-jump apparatus. Through the pressure-jump technique, Hachyia *et al.* (9, 10) verified exchange between protons and cations as a mechanism of surface adsorption. Hayes and Leckie (6) successfully integrated TLM and pressure-jump results in interpreting the mechanistic pathways of Pb sorption on goethite. Lately ad-

[1] To whom correspondence should be addressed.
[2] Visiting scholar.

0021-9797/98 $25.00

sorption kinetic work of trivalent cations was systematically overviewed by Chang *et al.* (11) and Lin *et al.* (12), who proposed different sorption pathways for divalent and trivalent ions.

In comparison to cation sorption kinetics, less work has been devoted to anion sorption kinetics. Mikami *et al.* (13, 14) studied the kinetics of chromate and phosphate adsorption onto γ-Al_2O_3 by the pressure-jump technique; Hachiya *et al.* (15) studied the adsorption mechanism of IO_3^- on γ-Al_2O_3; and Zhang and Sparks (16–18) focused on the mechanisms of oxyanion (molybdate, sulfate, selenate, and selenite) adsorption on goethite. Sorption of anions onto iron oxides surface were proposed to be a two-step pathways. Primarily, formation of outer-sphere complex and thereafter a transformation of outer-sphere complex to inner-sphere complex were verified by these kinetic work. It is interesting to note that arsenate and chromate exhibit a dramatically different sorption mechanisms from previous investigations by using same kinetic techniques (19). In this current work, it is intended to provide kinetic investigation on the molybdate/γ-Al_2O_3 sorption system using pressure-jump relaxation technique. The results should be useful in understanding adsorption mechanisms of oxyanion on mineral surface as well as in comparison sorption kinetics between iron oxide and aluminum oxide.

MATERIALS AND METHODS

Materials

Stock MoO_4^{2-} solution (2.5×10^{-2} M) was prepared with Na_2MoO_4 (reagent grade from Merck) and distilled/deionized water (Milli-Q SP). The background electrolyte $NaNO_3$ concentrations were adjusted to 0.01, 0.05, and 0.1 M. γ-Al_2O_3 (Aerosil Co., Japan) was purified by electrodialysis (1200 V, 3 mA) before use. The surface area of γ-Al_2O_3, determined by the manufacturer from N_2 Brunauer–Emmett–Teller adsorption isotherm, was equal to 100 m^2/g. Site density of 8 sites/nm^2 was chosen from the Peri's work (20). Reagent grade HNO_3 and NaOH were used for system pH adjustment.

Sorption Experiments

In batch equilibrium adsorption experiments, molybdate (5×10^{-3} M) was equilibrated with γ-Al_2O_3 suspension (30 g/L) in the presence of 0.01, 0.05, and 0.1 M $NaNO_3$, and the pH of the suspension was adjusted with a small amount of HNO_3 or NaOH to cover the range from pH 4.5 to 9. Samples were subjected to shaking for 24 h and kept at 25 $\pm$ 0.1°C. At the end of the equilibrium period, each suspension pH was determined. The suspension was centrifuged at 8000 rpm for 15 min, and the supernatant was then filtered through 0.2 μm filter paper (Gelman Sciences). Molybdate concentration was determined by ion chromatography (Dionex 2000i SP).

TABLE 1
TLM Parameters and Basic Surface Complexation Constants

C_1 (o-plane capacitance, μF/cm^2)	80 (23)
C_2 (β-plane capacitance, μF/cm^2)	20 (23)
log K_{a1}^{int}, log K_{a2}^{int}	−7.2, −9.5 (24)
log $K_{Na^+}^{int}$, log $K_{NO_3^-}^{int}$	−9.1, 8.7 (6, 18)

Kinetic Measurements

The pressure-jump apparatus was used for obtaining mechanistic information of MoO_4^{2-}/γ-Al_2O_3 interactions. The samples prepared in batch equilibrium experiments after pH measurement were saved for pressure-jump work. The temperature was maintained at 25 $\pm$ 0.1°C in both the sample cell and the reference cell (KCl solution). The pressure-jump apparatus was equipped with a conductivity detector and was similar to that used previously by Hachiya *et al.* (10). The primary components of the pressure-jump apparatus were a pressure chamber (Photo High Pressure Inc., Japan), a Wheatstone bridge circuit (Sea Land Electr. Wave Inc., Japan) and a digital storage oscilloscope (TEK 2224).

During the pressure-jump relaxation measurement, the equilibrium state of the MoO_4^{2-}/γ-Al_2O_3 system was perturbed by raising the system pressure to 100 atm using a camshaft pressure pump. The sample and reference cells were covered with a plastic membrane to transmit the pressure effectively. A piece of brass shimstock (thickness = 0.05 mm) was used for pressure control. The brass membrane burst when the pressure in the autoclave became too high and caused the pressure to return to ambient pressure within 100 μs. At the moment of pressure change, an oscilloscope was triggered to record the changes in system conductivity. The signals recorded by the oscilloscope were digitized and analyzed by linear regression to calculate the reciprocal relaxation time (τ^{-1}). The time necessary for the equilibrium adjustment to take place is called the relaxation time (τ), which is related to the rates of the reactions in the system (21).

Model Analysis

The TLM developed by Davis and Leckie (22) and subsequently modified by Hayes and Leckie (6) was used to simulate the equilibrium partitioning of background electrolyte ions and MoO_4^{2-} species at the γ-Al_2O_3/water interface. The modified TLM differs from the original model in two ways. First, the adsorbed ion can be located on both the o-layer and the β-layer, i.e., ions are allowed to form either inner- or outer-sphere surface complexes. Second, the chemical potential and standard and reference states are defined equivalently for both solution and surface species, leading to a different relationship between the activity coefficients and the interfacial potential than previously used. The reactions constants and other parameters necessary for TLM are summarized in Table 1. The equations for TLM simulation are presented below:

$$SOH_2^+ \rightleftharpoons SOH + H^+, \quad [1]$$

$$SOH \rightleftharpoons SO^- + H^+, \quad [2]$$

$$SOH + Na^+ \rightleftharpoons SO^- – Na^+ + H^+, \quad [3]$$

$$SOH + H^+ + NO_3^- \rightleftharpoons SOH_2^+ – NO_3^-, \quad [4]$$

$$SOH + H^+ + MoO_4^{2-} \rightleftharpoons SOH_2^+ – MoO_4^{2-}, \quad [5]$$

$$SOH + H^+ + MoO_4^{2-} \rightleftharpoons SMoO_4^- + H_2O, \quad [6]$$

$$2SOH + 2H^+ + MoO_4^{2-} \rightleftharpoons S_2MoO_4 + 2H_2O. \quad [7]$$

Equations [1] and [2] describe protonation of reacting surface sites, and Eqs. [3] and [4] describe the formation of complexes between the background electrolyte ions and the surface. Ion-pairs are formed at the β-plane (Eq. [5]), where the adsorption is nonspecific and the reaction product is an outer-sphere surface complex, if MoO_4^{2-} reacts similarly to a background electrolyte with SOH. If adsorption of MoO_4^{2-} is visualized as a chemically specific reaction, the reaction, however, can be expressed as an inner-sphere surface coordination process (Eqs. [6] and [7]). Equations [6] and [7] represent the reaction of MoO_4^{2-} with 1 and 2 mol of reactive surface hydroxyl to form inner-sphere monodentate and bidentate surface complexes, respectively.

The intrinsic conditional equilibrium constants for the previous reactions can be defined as

$$K_{a1}^{\text{int}} = \frac{[\overline{SOH}][\overline{H^+}]}{[\overline{SOH_2^+}]} \exp\left(\frac{-\psi_o F}{RT}\right) = 10^{-7.2}, \quad [8]$$

$$K_{a2}^{\text{int}} = \frac{[\overline{SO^-}][\overline{H^+}]}{[\overline{SOH}]} \exp\left(\frac{-\psi_o F}{RT}\right) = 10^{-9.5}, \quad [9]$$

$$K_{Na^+}^{\text{int}} = \frac{[\overline{SO^- - Na^+}][\overline{H^+}]}{[\overline{SOH}][\overline{Na^+}]} \exp\left(\frac{-(\psi_\beta - \psi_o) F}{RT}\right) = 10^{-9.1}, \quad [10]$$

$$K_{NO_3^-}^{\text{int}} = \frac{[\overline{SOH_2^+ - NO_3^-}]}{[\overline{SOH}][\overline{H^+}][\overline{NO_3^-}]} \exp\left(\frac{(\psi_o - \psi_\beta) F}{RT}\right) = 10^{8.7}, \quad [11]$$

$$K_{MoO_4^{2-}}^{\text{int}} = \frac{[\overline{SOH_2^+ - MoO_4^{2-}}]}{[\overline{SOH}][\overline{H^+}][\overline{MoO_4^{2-}}]} \exp\left(\frac{(\psi_o - 2\psi_\beta) F}{RT}\right), \quad [12]$$

$$K_{(MoO_4^{2-})^{*1}}^{\text{int}} = \frac{[\overline{SMoO_4^-}]}{[\overline{SOH}][\overline{H^+}][\overline{MoO_4^{2-}}]} \exp\left(\frac{-\psi_o F}{RT}\right), \quad [13]$$

$$K_{(MoO_4^{2-})^{*2}}^{\text{int}} = \frac{[\overline{S_2MoO_4}]}{[\overline{SOH}]^2[\overline{H^+}]^2[\overline{MoO_4^{2-}}]}, \quad [14]$$

where F is the Faraday constant, R is the universal gas constant, T is the absolute temperature, and ψ_o and ψ_β are the electrical potentials at the o- and β-plane, respectively. The equilibrium and mass balance equations are solved simultaneously in the TLM. The parameters of equations in Table 1 was used in the model analysis to determine the best-fit intrinsic constants for the MoO_4^{2-}/γ-Al_2O_3 reaction.

RESULTS AND DISCUSSIONS

Equilibrium Adsorption

The sorption envelope of 5×10^{-3} M molybdate on 30 g/L γ-Al_2O_3 in the absence of $NaNO_3$ and in the presence of three different $NaNO_3$ electrolyte concentrations (0.01, 0.05, and 0.1 M) are presented in Fig. 1. The pH dependent adsorption curve is similar to those of other anions; sorption density is increased with system pH shifting from alkaline to acidic conditions. Sorption envelopes of some anions normally exhibit a more flat curve over a extended acidic pH ranges such as arsenite and arsenate in iron oxide systems (25, 26). However, in this molybdate and γ-Al_2O_3 suspension, the sorption of molybdate changes from negligible amount to near-total removal in only about 3.5 pH units. It might be interesting to note that the sorption affinity of anions for the oxides can be reasoned by the positions of different pH–adsorption curves. Probably, highly adsorbable anions generally exhibit a flat sorption curve over a wider pH range. The maximum sorption density of molybdate in this current experimental condition is calculated to be 1.67×10^{-6} mol/m^2. For comparison, the sorption densities of chromate, selenite, selenate, arsenite, and arsenate are 2×10^{-6} mol/m^2 on goethite and 10^{-6} mol/m^2 on goethite and 10^{-6} mol/m^2 on γ-Al_2O_3, 3.04×10^{-6} mol/m^2 on goethite, 1.23×10^{-5} mol/m^2 on ferrihydrite, and 2×10^{-6} mol/m^2 on goethite and 5.11×10^{-6} mol/m^2 on ferrihydrite, respectively (13, 18, 19, 26).

The effect of background electrolyte concentrations on molybdate adsorption at a given pH is fairly insignificant as shown in Fig. 1. The insignificance of electrolyte ionic strength on molybdate sorption might imply the formation of inner-sphere surface complex, which can be verified by the TLM simulation. Thus, the formation of different outer- and inner-sphere complexes of molybdate as proposed in Eqs. [5]–[7] was modeled using adsorption data with no $NaNO_3$ addition. The formation of an outer-sphere complex was fairly impossible as the TLM simulation was unable to coincide the experimentally measured pH–adsorption curve. The TLM was, however, able to follow the experimental pattern well for the formation of inner-sphere complexes of monodentate $SMoO_4^-$ (Eq. [6]) and bidentate S_2MoO_4 (Eq. [7]) as shown in Fig. 1. The fitted intrinsic formation constants for the $SMoO_4^-$ and S_2MoO_4 are $10^{6.5}$ M^{-2} and 10^{16} M^{-4}, respectively. The equilibrium constants and the assumption of inner-sphere surface complexes are to be further verified using the kinetic methods. If the intrinsic

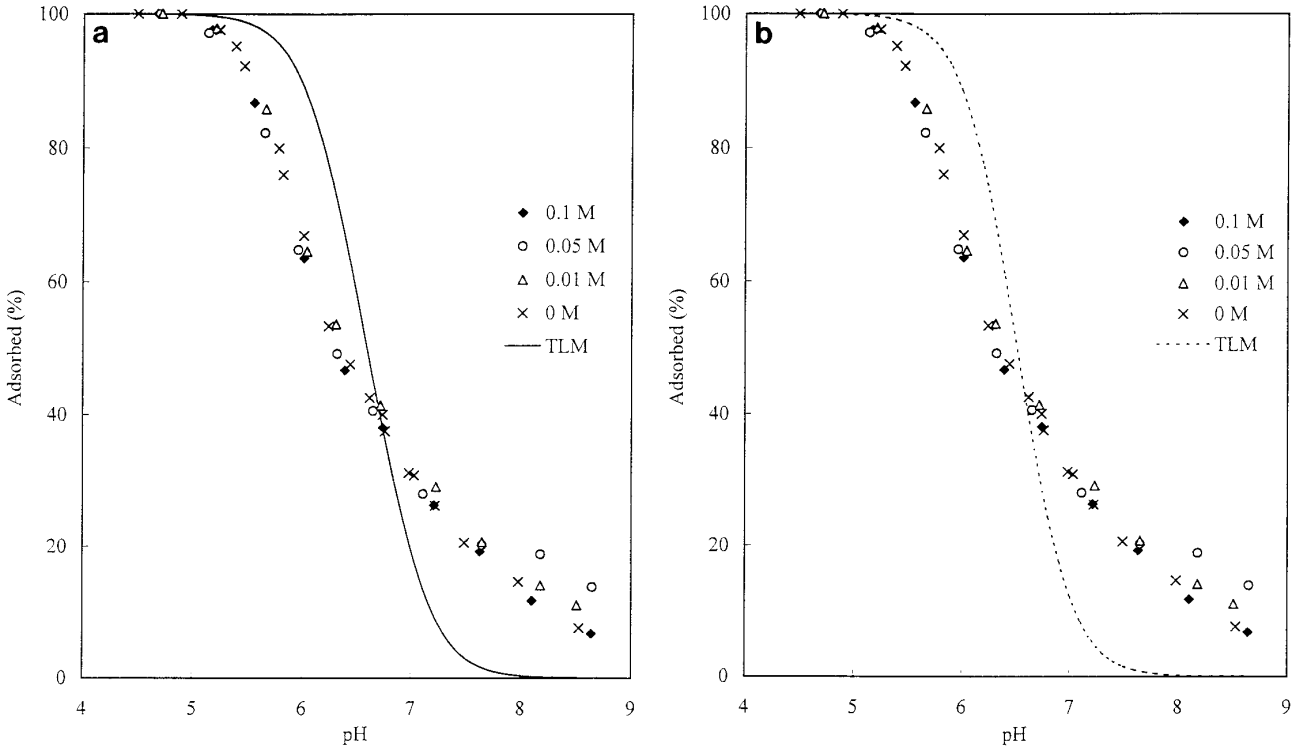

FIG. 1. Adsorption of MoO_4^{2-} onto γ-Al_2O_3 as a function of pH at various background $NaNO_3$ concentrations. (a) TLM (Eq. [6]) for solid curve, and (b) TLM (Eq. [7]) for dotted curve. Symbols denote experimental data.

equilibrium constants derived from the kinetic rate constants are comparable, one is able to ascertain the surface complex configuration and the adsorption mechanisms.

Kinetic Studies

The pressure-jump technique was used to elucidate the adsorption mechanism proposed by the equilibrium studies and to provide rate constants for both adsorption and desorption reactions. The kinetics of MoO_4^{2-} adsorption on γ-Al_2O_3 using the pressure-jump apparatus with a conductivity detector revealed a double relaxation (not shown), indicating a fast reaction step and a slow reaction step (Fig. 2). To ensure that the relaxation was solely a result of the perturbation on equilibrated γ-Al_2O_3 suspension MoO_4^{2-}, different systems, containing supernatant from the MoO_4^{2-}/γ-Al_2O_3 suspension, γ-Al_2O_3 alone, and Na_2MoO_4, were also subjected to the same pressure-jump test as that for the MoO_4^{2-}/γ-Al_2O_3 suspension. No relaxation was observed in any of the above systems except for the supernatant system, which was different from previous studies of cations and anions (11–14, 16–18, 27). Since the diameter of a γ-Al_2O_3 particle is about 13 nm, a portion of the particles could not be removed when the suspension was centrifuged at 8000 rpm. As a result, the trace amount of γ-Al_2O_3 particles left in the supernatant solutions caused a slow relaxation. Unfortunately, we did not monitor relaxation in the filtrate system. Since the sweep velocity of the supernatant in the pressure-jump test is 1 s/div (which is a very slow relaxation), the effect of the relaxation is negligible. On the other hand, the sweep velocity for MoO_4^{2-}/γ-Al_2O_3 suspension in the pressure-jump test is 0.1 s/div which is a fast relaxation. The result indicates that the relaxation of the suspension is ten times faster than that of the supernatant. Therefore, the effect of supernatant relaxation was considered to be neglible, and it should be justified to assume that relaxation is attributed solely to the adsorption/desorption of MoO_4^{2-} at the water/γ-Al_2O_3 interface. Hence, the reciprocal relaxation times of the fast step (τ_f^{-1}) and the slow step (τ_s^{-1}) could be calculated from semilog plots of the relaxation curves. The measured reciprocal relaxation times are shown in Fig. 3. Both τ_f^{-1} and τ_s^{-1} increased with increasing pH of the MoO_4^{2-}/γ-Al_2O_3 suspension, although τ_s^{-1} is less dependent upon pH.

Based on the results from the pressure-jump studies as well as from the equilibrium experiments, two-step reactions are postulated to describe the reaction steps of MoO_4^{2-} adsorption onto γ-Al_2O_3. Proposed reaction pathways, the relationship between reciprocal relaxation times and reactant and product concentrations, and the linearized relationships are presented in the following equations. Specifically, the proposed following reaction mechanisms are derived from the batch results indi-

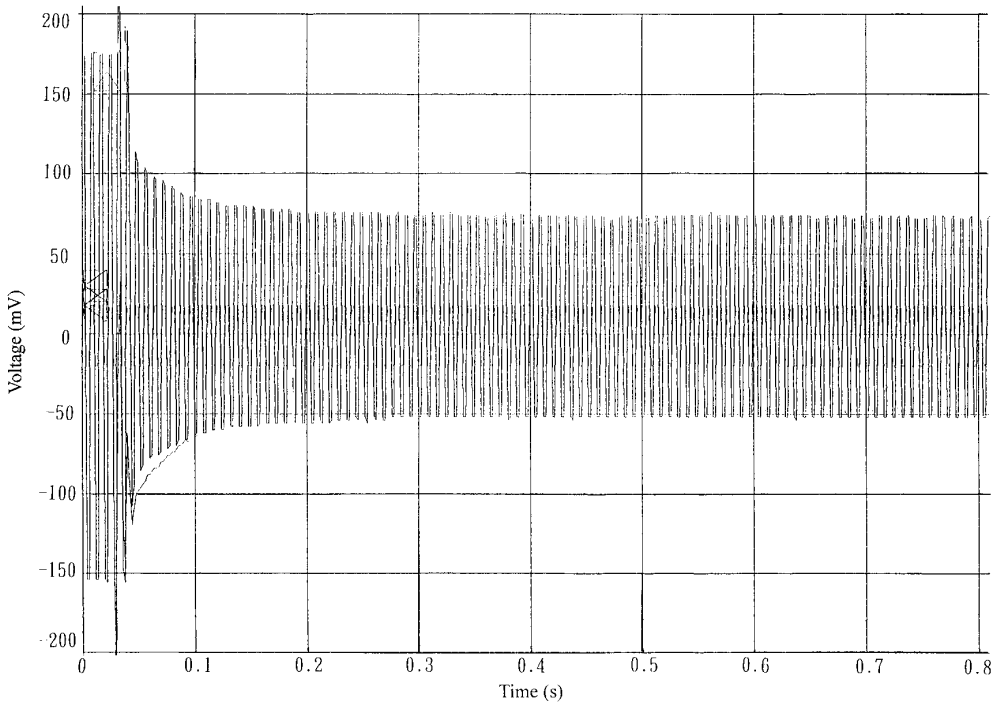

FIG. 2. Typical relaxation curve in the $MoO_4^{2-}/\gamma\text{-}Al_2O_3$ system using the pressure-jump technique at pH 6.01, sweep = 0.1 s/div, and 25°C.

cating that mono- or bidentate inner-sphere complexes are formed in the $MoO_4^{2-}/\gamma\text{-}Al_2O_3$ system:

$$SOH + H^+ + MoO_4^{2-} \underset{k_{-1}}{\overset{k_1}{\rightleftharpoons}} SOH_2^+\text{–}MoO_4^{2-}, \qquad [15]$$

$$SOH_2^+\text{–}MoO_4^{2-} \underset{k_{-2}}{\overset{k_2}{\rightleftharpoons}} SMoO_4^- + H_2O. \qquad [16]$$

If Eq. [15] is a faster step than Eq. [16], the relationship between reciprocal relaxation time and reactant and product concentrations is represented by Eqs. [17] and [18] (see derivations in the Appendix):

$$\frac{1}{\tau_f}\exp\left(\frac{(2\psi_\beta - \psi_o)F}{2RT}\right) = k_1^{int}\left\{\exp\left(\frac{(2\psi_\beta - \psi_o)F}{RT}\right)([\overline{SOH}][\overline{H^+}] + [\overline{SOH}][\overline{MoO_4^{2-}}] + [\overline{H^+}][\overline{MoO_4^{2-}}])\right\} + k_{-1}^{int} = k_1^{int}\{MI^*\} + k_{-1}^{int}, \qquad [17]$$

$$\frac{1}{\tau_s}\exp\left(\frac{(\psi_o - \psi_\beta)F}{RT}\right) = k_2^{int}\left\{\frac{K_1^{int}\exp\left(\frac{\psi_o F}{RT}\right)([\overline{SOH}][\overline{H^+}] + [\overline{SOH}][\overline{MoO_4^{2-}}] + [\overline{H^+}][\overline{MoO_4^{2-}}])}{1 + K_1^{int}(MI^*)}\right\} + k_{-2}^{int} = k_2^{int}\{MI^{**}\} + k_{-2}^{int}. \qquad [18]$$

The alternative proposed adsorption mechanisms are expressed in Eqs. [19] and [20] for the formation of bidentate inner-sphere complex. When Eq. [19] is assumed to be a fast step or a slow step, the relationship between the reciprocal relaxation times and the reactant and product concentrations can be also derived. The k_1^{int}, k_{-1}^{int}, k_2^{int}, and k_{-2}^{int} are the intrinsic forward (k_1^{int} and k_2^{int}) and backward (k_{-1}^{int} and k_{-2}^{int}) rate constants for steps 1 and 2, respectively:

$$2SOH + 2H^+ + MoO_4^{2-} \underset{k_{-1}}{\overset{k_1}{\rightleftharpoons}} (SOH_2^+)_2\text{–}MoO_4^{2-}, \qquad [19]$$

$$(SOH_2^+)_2\text{–}MoO_4^{2-} \underset{k_{-2}}{\overset{k_2}{\rightleftharpoons}} S_2MoO_4 + 2H_2O. \qquad [20]$$

To examine the plausibility of the proposed adsorption mechanisms, the corresponding reciprocal relaxation times were derived as a function of the reactant and product concentrations for the postulated mechanisms. If a plot of τ_f^{-1} (or τ_s^{-1}) measured by pressure-jump apparatus versus the corresponding {M*} (or {M**}) functions calculated by TLM is linear, the hypothesized mechanism is consistent with the data. The intrinsic reaction rate constants can be determined from the slope and/or intercept of such a plot.

Examining the plots of reciprocal relaxation times (τ_f^{-1} and τ_s^{-1}) versus the expression of reactant and product concentrations, it is found that only Eqs. [17] and [18] yield good linearity (Figs. 4 and 5), confirming that the surface reaction of the $MoO_4^{2-}/\gamma\text{-}Al_2O_3$ system can be well described by the proposed fast and slow steps. Although both models of mono- and bidentate inner-sphere complex formations appear to be true in batch results (Fig. 1a and

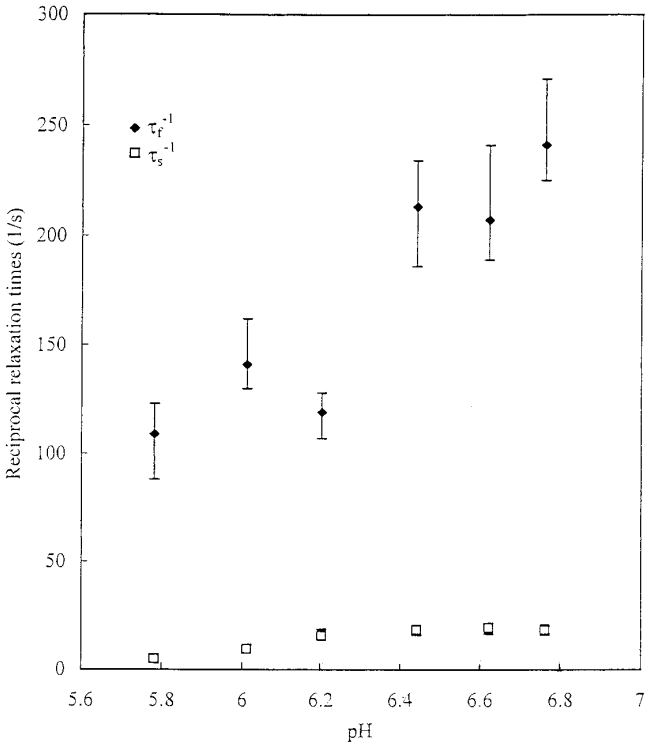

FIG. 3. Double reciprocal relaxation times (τ_f^{-1}, τ_s^{-1}) as a function of pH in the MoO_4^{2-}/γ-Al_2O_3 system.

1b), the kinetic analysis, however, indicates that the adsorption/desorption of MoO_4^{2-} is caused only by monodentate inner-sphere complex formation. The results presented in Fig. 4 indicate that the surface reaction sites first react with H^+ and MoO_4^{2-} to form an outer-sphere complex. Thereafter outer-sphere complex releases one water molecule to form an inner-sphere complex, which is clearly evident by Fig. 5. The respective kinetic values of the intrinsic forward rate and reverse rate constants calculated from the slope and intercept in Figs. 4 and 5 are summarized in Table 2. The equilibrium constants obtained from kinetic experiment ($K_{kin}^{int} = 10^6\ M^{-2}$) is in good agreement with the results from equilibrium and TLM work ($K_{eq}^{int} = 10^{6.5}\ M^{-2}$), confirming that the mechanism of MoO_4^{2-} adsorption/desorption onto γ-Al_2O_3 can be interpreted by Eqs. [15] and [16].

This study provides especial evidence to show that MoO_4^{2-} adsorption onto γ-Al_2O_3 is a two-step reaction; the first step is the formation of an ion-pair complex between the sites and MoO_4^{2-}, and the second step is a ligand exchange process. Based on the relaxation theory and with the help of pressure-jump technique, the microscopic insight of the adsorption pathways of trace elements on Fe or Al oxide/hydroxide can be elucidated thoughtfully. Our past studies on the sorption mechanism of cations reveal that inner-sphere surface complexes always involve a two-step ligand exchange reaction at the interface. However, the exchange steps of a divalent cation are not similar to a trivalent cation (12) in that the role of hydration water molecules are significantly different. Divalent cation forms inner-sphere species and loses a hydrated water molecule simultaneously in the first step, and the second step is the release of a proton from the surface hydroxyl OH group. Alternatively, trivalent cation is to form a outer-sphere surface complex without losing any hydrated water molecule first, followed by the detachment of a H_2O to form the inner-sphere surface species. Examining the kinetic results in this work, it is found that the microscopic reaction steps of molybdate on γ-Al_2O_3 is somewhat analogous to those of trivalent cation. In both situations, trivalent ions and oxyanions all react with surface site to form outer-sphere complexes and thereafter shifting to form inner-sphere complexes. By further evaluating the sorption mechanisms of these three different ions, one might come to a conclusion that sorption pathways of ions with extensive degree of hydration as trivalent cations and oxyanions are in the category of associative process or are analogous to the mechanism of the substitution nucleophilic unimolecular (28). This finding is further supported by the work of Zhang and Spark (16) on the kinetics and mechanisms of MoO_4^- sorption on goethite. In their study, an ion-pair of molybdate is first to form at the goethite surface through the electrostatic interaction. The second step is postulated as the ligand exchange of molybdate with H_2O to form an inner-sphere complex. It is also interesting to note that although molybdate oxyanion exhibit a similar reaction mechanism at the goethite and γ-Al_2O_3 interfaces, there exists a greater discrepancy between the kinetic rate constants. In all the reaction steps, the molybdate/γ-Al_2O_3 system has a much smaller reverse rate constants (k_{-1}) than those of the molybdate/goethite system (Table

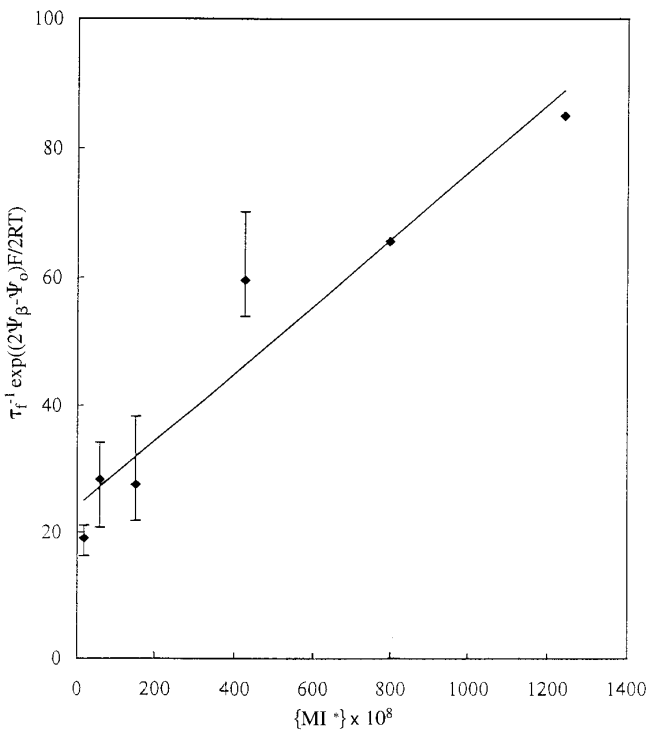

FIG. 4. Plot of $\tau_f^{-1}\exp((2\psi_\beta - \psi_o)F/2RT)$ vs {MI*} in Eq. [17]. The concentrations of MoO_4^{2-} species were calculated on the basis of the optimized intrinsic formation constants.

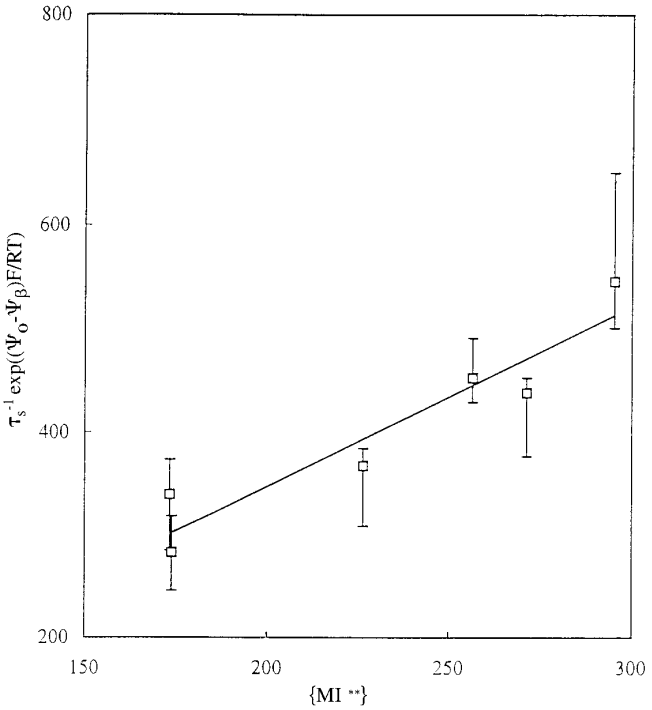

FIG. 5. Plot of $\tau_s^{-1}\exp((\psi_o - \psi_\beta)F/RT)$ vs {MI**} in Eq. [18]. The concentration of MoO_4^{2-} species was calculated based on the optimized intrinsic formation constants.

2). This comparison indicates that molybdate is more labile at the goethite/water interface than at the γ-Al_2O_3/water interface.

CONCLUSIONS

Adsorption data and TLM simulation reveal that the adsorption of MoO_4^{2-} onto γ-Al_2O_3 forms an inner-sphere surface complex. The pressure-jump technique was used to examine the adsorption kinetics and verify the reaction steps. The proposed adsorption mechanism is a two-step process forming an inner-sphere surface complex. The first step involves the initiation of MoO_4^{2-} and H^+ to form an outer-sphere surface complex, and the subsequent step is a ligand exchange reaction, which results in the formation of an inner-sphere monodentate surface complex. The sorption pathways are similar to those of trivalent cations, which categorized as associative processes. Both equilibrium and kinetic data fit the proposed mechanism for the reaction steps and TLM well. Furthermore, this study indicates that the adsorption of MoO_4^{2-} on γ-Al_2O_3 is more stable than the adsorption of MoO_4^{2-} on goethite.

APPENDIX

From Eqs. [15] and [16], the species can be defined as A = SOH, B = H^+, C = MoO_4^{2-}, D = SOH_2^+–MoO_4^{2-}, E = $SMoO_4^-$, and F = H_2O. The general forms of the adsorption/desorption reactions are

$$A + B + C \underset{k_{-1}}{\overset{k_1}{\rightleftharpoons}} D \text{ (step 1, fast)}, \qquad [A.1]$$

$$D \underset{k_{-2}}{\overset{k_2}{\rightleftharpoons}} E + F \text{ (step 2, slow)}. \qquad [A.2]$$

The rate of step 1 is defined as

$$-\frac{dC_A}{dt} = k_1 C_A C_B C_C - k_{-1} C_D. \qquad [A.3]$$

At equilibrium, $dC_A/dt = 0$ and then Eq. [A.3] becomes

$$k_1 \overline{C_A C_B C_C} = k_{-1} \overline{C_D}, \qquad [A.4]$$

where the overbar denotes the equilibrium concentration. Following a small perturbation equilibrium concentrations are shifted by a small amount, x.

$$\begin{aligned} -\frac{dC_A}{dt} &= -\frac{d(\overline{C_A} + x)}{dt} \\ &= k_1(\overline{C_A} + x)(\overline{C_B} + x)(\overline{C_C} + x) - k_{-1}(\overline{C_D} - x) \\ &= k_1 \overline{C_A C_B C_C} - k_{-1}\overline{C_D} + [k_1(\overline{C_A C_B} + \overline{C_A C_C} + \overline{C_B C_C}) \\ &\quad + k_{-1}]x + k_1[\overline{C_A} + \overline{C_B} + \overline{C_C}]x^2 + k_1 x^3, \end{aligned} \qquad [A.5]$$

which can be further simplified if only small equilibrium

TABLE 2
Intrinsic Rate and Equilibrium Constants Determined from Kinetic Measurements[a]

	k_1^{int}	k_{-1}^{int}	k_2^{int}	k_{-2}^{int}	K_1^{int}	K_2^{int}	K_{kin}^{int}	K_{eq}^{int}
(I)	$M^{-2}\ s^{-1}$	s^{-1}	s^{-1}	s^{-1}	M^{-2}		M^{-2}	M^{-2}
	5.2×10^6	2.4×10	1.7	3.6×10^{-1}	2.2×10^5	4.8	1.0×10^6	3.2×10^6
(II)	$M^{-1}\ s^{-1}$	s^{-1}	$M^{-1}\ s^{-1}$	s^{-1}	M^{-1}	M^{-1}	M^{-2}	M^{-2}
	4.0×10^3	3.9×10^2	1.9	42.3	1.0×10	4.5×10^{-2}	4.6×10^{-1}	–

[a] (I), present work; (II), Zhang and Sparks (16).

perturbations are considered. Consequently, x^2 and x^3 become increasingly small, leading to

$$-\frac{dx}{dt} = [k_1(\overline{C_A C_B} + \overline{C_A C_C} + \overline{C_B C_C}) + k_{-1}]x. \quad [A.6]$$

Since Bernasconi [21] proved that

$$\frac{dx}{dt} = -\frac{x}{\tau}. \quad [A.7]$$

Equation [A.6] can be written as

$$\frac{1}{\tau_f} = k_1(\overline{C_A C_B} + \overline{C_A C_C} + \overline{C_B C_C}) + k_{-1}. \quad [A.8]$$

Combining the following relationships based on Eq. [A.1]

$$k_1 = k_1^{int}\exp\left(\frac{(2\psi_\beta - \psi_o)F}{2RT}\right), \quad [A.9]$$

$$k_{-1} = k_{-1}^{int}\exp\left(\frac{(\psi_o - 2\psi_\beta)F}{2RT}\right). \quad [A.10]$$

Equation [A.8] becomes

$$\frac{1}{\tau_f}\exp\left(\frac{(2\psi_\beta - \psi_o)F}{2RT}\right) = k_1^{int}\exp\left(\frac{(2\psi_\beta - \psi_o)F}{RT}\right) \times (\overline{C_A C_B} + \overline{C_A C_C} + \overline{C_B C_C}) + k_{-1}^{int} = k_1^{int}\{MI^*\} + k_{-1}^{int}. \quad [A.11]$$

The equilibrium constant of step 1 (K_1) can be defined as

$$K_1 = \frac{\overline{C_D}}{\overline{C_A C_B C_C}} = \frac{C_D}{C_A C_B C_C} = \frac{(\overline{C_D} + \Delta C_D)}{(\overline{C_A} + \Delta C_A)(\overline{C_B} + \Delta C_B)(\overline{C_C} + \Delta C_C)}. \quad [A.12]$$

Rerranging [A.12] as

$$\overline{C_D} + \Delta C_D = K_1(\overline{C_A} + \Delta C_A)(\overline{C_B} + \Delta C_B)(\overline{C_C} + \Delta C_C), \quad [A.13]$$

with a small perturbation,

$$\overline{C_A}\Delta C_B \Delta C_C \approx 0, \quad [A.14]$$

$$\overline{C_B}\Delta C_A \Delta C_C \approx 0, \quad [A.15]$$

$$\overline{C_C}\Delta C_A \Delta C_B \approx 0, \quad [A.16]$$

$$\Delta C_A \Delta C_B \Delta C_C \approx 0. \quad [A.17]$$

Substituting Eqs. [A.14]–[A.17] into Eq. [A.13] yields

$$\Delta C_D = K_1(\overline{C_B C_C}\Delta C_A + \overline{C_A C_C}\Delta C_B + \overline{C_A C_B}\Delta C_C). \quad [A.18]$$

The conservation-of-mass law states that

$$\Delta C_A = \Delta C_B = \Delta C_C, \quad [A.19]$$

$$\Delta C_D = -\Delta C_A - \Delta C_E. \quad [A.20]$$

When Eqs. [A.19] and [A.20] are substituted into Eq. [A.18], the following equation is obtained:

$$\Delta C_D = \frac{-K_1(\overline{C_A C_B} + \overline{C_B C_C} + \overline{C_A C_C})}{1 + K_1(\overline{C_A C_B} + \overline{C_B C_C} + \overline{C_A C_C})}\Delta C_E \quad [A.21]$$

The rate of step 2 is defined as:

$$\frac{dC_E}{dt} = \frac{d(\overline{C_E} + \Delta C_E)}{dt} = k_2(\overline{C_D} + \Delta C_D) - k_{-2}(\overline{C_E} + \Delta C_E). \quad [A.22]$$

Combining Eq. [A.21] and Eq. [A.22] gives

$$\frac{d\Delta C_E}{dt} = -\left[\frac{k_2 K_1(\overline{C_A C_B} + \overline{C_B C_C} + \overline{C_A C_C})}{1 + K_1(\overline{C_A C_B} + \overline{C_B C_C} + \overline{C_A C_C})} + k_{-2}\right]\Delta C_E. \quad [A.23]$$

Using the definition of relaxation time (Eq. [A.7]), Eq. [A.23] becomes

$$\frac{1}{\tau_s} = \frac{k_2 K_1(\overline{C_A C_B} + \overline{C_B C_C} + \overline{C_A C_C})}{1 + K_1(\overline{C_A C_B} + \overline{C_B C_C} + \overline{C_A C_C})} + k_{-2}. \quad [A.24]$$

Considering the effect of the double electrostatic layer from Eqs. [15] and [16],

$$K_1 = K_1^{int}\exp\left(\frac{(2\psi_\beta - \psi_o)F}{RT}\right), \quad [A.25]$$

$$k_2 = k_2^{int}\exp\left(\frac{(\psi_o - \psi_\beta)F}{RT}\right), \quad [A.26]$$

$$k_{-2} = k_{-2}^{int}\exp\left(\frac{(\psi_\beta - \psi_o)F}{RT}\right). \quad [A.27]$$

Substitution of Eqs. [A.25]–[A.27] into Eq. [A.24] gives

$$\frac{1}{\tau_s}\exp\left(\frac{(\psi_o - \psi_\beta)F}{RT}\right) = k_2^{int}\left\{\frac{K_1^{int}\exp\left(\frac{\psi_o F}{RT}\right)(\overline{C_A C_B} + \overline{C_B C_C} + \overline{C_A C_C})}{1 + K_1^{int}\exp\left(\frac{(2\psi_\beta - \psi_o)F}{RT}\right) \times (\overline{C_A C_B} + \overline{C_B C_C} + \overline{C_A C_C})}\right\} + k_{-2}^{int} = k_2^{int}\{MI^{**}\} + k_{-2}^{int}. \quad [A.28]$$

When the defined species are converted into reactants in Eqs. [A.11] and [A.28], Eqs. [17] and [18] are obtained, respectively.

ACKNOWLEDGMENTS

The authors thank Professor Olive J. Hao, University of Maryland, for the valuable discussions and the reviewers for their constructive comments. Funding for this research was provided by the National Science Council of the Republic of China under Grant NSC 83-0410-E-002-082.

REFERENCES

1. Parker, G. A., "Analytical Chemistry of Molybdenum." Springer-Verlag, Berlin, Germany, 1983.
2. Windholz, M., Budavari, S., Blumetti, R. F., and Otterbein, E. S., "The Merck Index," 10th ed. Merck Sharp & Dohme Research Laboratories, Rahway, NJ, 1983.
3. Bodek, I., Lyman, W. J., Reehl, W. F., and Rosenblatt, D. H., "Environmental Inorganic Chemistry." Pergamon Press, New York, 1988.
4. Stumm, W., Huang, C. P., and Jenkins, S. R., *Croat. Chem. Acta* **42,** 223–244 (1970).
5. Davis, J. A., and Leckie, J. O., *J. Colloid Interface Sci.* **67,** 90–107 (1978).
6. Hayes, K. F., and Leckie, J. O., *J. Colloid Interface Sci.* **115,** 564–572 (1987).
7. Pankow, J. F., and Morgan, J. J., *Environ. Sci. Technol.* **15,** 1155–1164 (1981).
8. Ogwada, R. A., and Sparks, D. L., *Soil Sci. Soc. Am. J.* **50,** 1158–1162 (1986).
9. Hachiya, K., Ashida, M., Sasaki, M., Kan, H., Inoue, T., and Yasunaga, T., *J. Phys. Chem.* **83,** 1866–1871 (1979).
10. Hachiya, K., Sasaki, M., Ikeda, T., Mikami, N., and Yasunaga, T., *J. Phys. Chem.* **88,** 27–31 (1984).
11. Chang, K. S., Lin, C. F., Lee, D. Y., Lo, S. L., and Yasunaga, T., *J. Colloid Interface Sci.* **165,** 169–176 (1994).
12. Lin, C. F., Chang, K. S., Tsay, C. W., Lee, D. Y., Lo, S. L., and Yasunaga, T., *J. Colloid Interface Sci.* **188,** 201–208 (1997).
13. Mikami, N., Sasaki, M., Klkuchi, T., and Yasunaga, T., *J. Phys. Chem.* **87,** 5245–5248 (1983).
14. Mikami, N., Sasaki, M., Hachiya, K., Astumian, R. D., Ikeda, T., and Yasunaga, T., *J. Phys. Chem.* **87,** 1454–1458 (1983).
15. Hachiya, K., Ashida, M., Sasaki, M., Karasuda, M., and Yasunaga, T., *J. Phys. Chem.* **84,** 2292–2296 (1980).
16. Zhang, P. C., and Sparks, D. L., *Soil Sci. Soc. Am. J.* **53,** 1028–1034 (1989).
17. Zhang, P. C., and Sparks, D. L., *Soil Sci. Soc. Am. J.* **54,** 1266–1273 (1990).
18. Zhang, P. C., and Sparks, D. L., *Environ. Sci. Technol.* **24,** 1848–1856 (1990).
19. Grossl, P. R., Eick, M., Sparks, D. L., Goldberg, S., and Ainsworth, C. C., *Environ. Sci. Technol.* **31,** 321–326 (1997).
20. Peri, J. B., *J. Phys. Chem.* **69,** 211–219 (1965).
21. Bernasconi, C. F., "Relaxation Kinetics." Academic Press, New York, 1976.
22. Davis, J. A., and Leckie, J. O., *J. Colloid Interface Sci.* **74,** 32–43 (1980).
23. Hayes, K. F., Redden, G., Ela, W., and Leckie, J. O., *J. Colloid Interface Sci.* **142,** 448–469 (1991).
24. Hohl, M., and Stumm, W., *J. Colloid Interface Sci.* **55,** 281–288 (1976).
25. Hsia, T. H., Lo, S. L., and Lin, C. F., *Chemosphere* **25,** 1825–1837 (1992).
26. Raven, K. P., Jain, A., and Loeppert, R. H., *Environ. Sci. Technol.* **32,** 344–349 (1998).
27. Chang, K. S., Lin, C. F., Lee, D. Y., and Lo, S. L., *Chemosphere* **27,** 1397–1407 (1993).
28. March, J., "Advanced Organic Chemistry: Reactions, Mechanism, and Structure." McGraw-Hill, New York, 1968.